Article

Impacts of Neighboring Buildings on the Cold Island Effect of Central Parks: A Case Study of Beijing, China

Dongrui Han [1,2], **Xiaohuan Yang [1,2,*]**, **Hongyan Cai [1]** and **Xinliang Xu [1]**

[1] State Key Laboratory of Resources and Environmental Information System, Institute of Geographic Sciences and Natural Resources Research, Chinese Academy of Sciences, Beijing 100101, China; handr@lreis.ac.cn (D.H.); caihy@lreis.ac.cn (H.C.); xuxl@lreis.ac.cn (X.X.)

[2] University of Chinese Academy of Sciences, Beijing 100049, China

* Correspondence: yangxh@lreis.ac.cn; Tel.: +86-10-6488-8608

Abstract: Urban parks have been considered as an effective measure to mitigate the urban heat island (UHI) effects. Many studies have investigated the impacts of shape, size and interior components on the cold island effect (CIE) of parks, while little attention has been given to the impact of neighboring buildings. Thus, taking twenty-two parks in Beijing as samples, this study investigated the impacts of the neighboring building on the CIE of central parks. The results showed that the average land surface temperature (LST) of parks are 30.98 °C in summer and −1.10 °C in winter. Parks have a strong CIE in summer, and average cold island footprint (CIF) and LST difference are 0.15 km^2 and 2.01 °C higher than that in winter. The components of the building in the CIF of parks are dominated by middle-rise building (MRB), followed by low-rise building (LRB), and high-rise building (HRB) is the least dominant. The percentage of landscape (PLAND) and landscape shape index (LSI) of MRB, and perimeter area fractal dimension (PAFRAC) of LRB are significantly related to CIF in summer and winter. This study could extend scientific understanding of the impacts of neighboring buildings on the CIE of central parks, and could guide urban planners in mitigating the UHI effects through the rational allocation of buildings.

Keywords: building; urban park; cold island effect; urban heat island

1. Introduction

Urbanization transforms the natural surface into impervious surface, while a high population in urban area accelerates this transformation [1–3]. This transformation was considered as one of the major causes for the phenomenon of urban heat island (UHI) [4,5]. The UHI refers to urban temperatures being higher than those in rural areas [6]. This negatively affects the quality and health of inhabitants [7,8]. Thus, how to mitigate the UHI effects has attracted wide concern from scholars and government managers.

The urban thermal environment has been extensively investigated by scholars, and the UHI effects is influenced by many factors [9–12]. It is widely accepted that greater absorption of solar radiation, lower efficiency of longwave radiation emission, energy storage by buildings and paved surface, lower evaporative cooling, and anthropogenic heat release in the urban area together lead to the UHI effects [13]. In addition, many studies have investigated relationships between urban (e.g., water bodies, roads, and built-up areas) and geographic (e.g., Normalized Difference Vegetation Index (NDVI), Normalized Difference Built-up Index (NDBI), and Normalized Difference Water Index (NDWI)) indicators and urban thermal environment [8,14–18]. Most of the existing research emphasized that built-up areas could increase the UHI effects, while water bodies and vegetation lands decrease it [1,17,19,20].

Urban parks, which mainly consist of grasses, trees, and water, are effective measures to mitigate the UHI effects [14,21–23]. They not only reduce the interiors' temperature, but also reduce the surrounding area's temperature [24]. The UHI mitigation improvement achieved by urban parks also attracted the attention of many scholars [21,25–29]. Several scholars have investigated the relationship between park size and the cold island effect (CIE) based on site data and remote sensing data, noting that the CIE is stronger as the park size increases [24,30]. Park shape also affects the land surface temperature (LST) of the park [24]. Generally, the more compact the shape, the better the CIE of the park [24,31]. Moreover, many scholars have pointed out that the CIE of the park is not only influenced by size and shape, but is also related to the interior landscape components [31,32]. Xu et al. (2017) emphasized that different landscape compositions and configurations of parks can affect the LST, and water bodies ratio and woodlands aggregation are considered to be the key influencing factors [24]. Furthermore, the CIE of the park is influenced by the characteristics of the area around the park [33,34]. Lin et al. (2015) investigated the cooling extent of parks in Beijing, and pointed out that the characteristics of the area around the park is also a key factor affecting the CIE of the parks [33]. Dai et al. (2018) also pointed out that landscape factors can affect the LST within or around parks [34]. However, although many studies have investigated the relationship between shape, size and interior components and the CIE of parks, the impact of the neighboring landscape on the CIE of parks is still lacking.

Due to data availability, current research explored the influence of the surrounding two-dimensional surface elements, such as impervious surface and built-up areas, but little attention has been paid to three-dimensional surface elements, such as buildings. Fortunately, the development of high-resolution remote sensing imagery and Light Detection And Ranging (LiDAR) enables the requirement of building data, including building outline and height [35,36]. These data could provide data support for exploring the impacts of building on thermal environment [37]. They could also provide fundamental data for investigating the impacts of neighboring buildings on the CIE of parks.

Most of the existing research has pointed out that buildings have different effects on LST [38]. Buildings can affect LST by modifying the surface characteristics and regional radiation energy balance [20,38–40]. Buildings with different height and form also have different effects on LST [29,41,42]. However, it is unclear that the impacts of the neighboring buildings (especially different types of buildings) on the CIE of parks. Thus, the impacts of neighboring buildings on the CIE of parks need to be investigated.

The objects of this study were (1) to investigate the LST difference among different parks; (2) to analysis the cool island footprint (CIF) of parks; (3) to further examine the composition of building neighboring parks; (4) to analyze LST difference between park and CIF; and (5) to investigate the effect of neighboring buildings on the CIE of parks. This study could provide guidance to urban planners on how to mitigate the UHI effects through the rational allocation of buildings.

2. Materials and Methods

2.1. Study Area

Beijing, the capital of China, is located in the northern of the country (39°26'–41°03' N, 115°25'–117°30' E). It covers an area of 164,100 km^2, with a population of 21.71 million as of 2015 (Figure 1). This region has a typical warm-temperate, semi-humid continental monsoon climate, with hot and rainy weather in summer and a cold and dry winter. The annual mean temperature and precipitation are 12.3 °C, and 300 to 800 mm, respectively. Beijing has experienced rapid urbanization since the 1978 economic reform and opening up policy. It is also one of the cities with serious UHI effects in China. The study area is located within the 3rd ring road of Beijing metropolitan area, which covers an area of approximately 80,000 km^2 (Figure 1). There are also many parks inside this region. Twenty-two parks were chosen to investigate the impacts of neighboring buildings on the CIE of central parks.
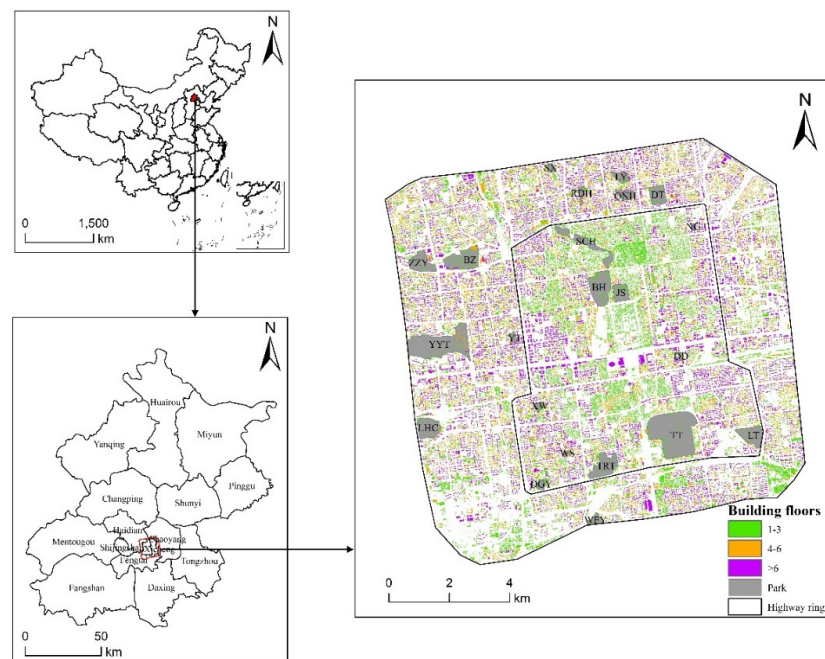
Figure 1. Location of the study area.

The spatial distribution and details of parks can see in Figure 1 and Table 1, respectively. Eleven parks are distributed in the 2nd ring, and the others are distributed in the 3rd ring. The area of parks ranged from 0.04 km^2 (WS) to 1.95 km^2 (TT), with an average area of 0.39 km^2.

Table 1. Characteristics of parks.

Name	Abbreviation	Latitude (°)	Longitude (°)	Area (km^2)
Beihai	BH	39.93	116.38	0.68
Beijing Zoo	BZ	39.94	116.33	0.66
Daguanyuan	DGY	39.87	116.35	0.09
Ditan	DT	39.95	116.41	0.32
Dongdan	DD	39.90	116.41	0.05
Jingshan	JS	39.92	116.39	0.28
Lianhuachi	LHC	39.89	116.31	0.46
Liuyin	LY	39.96	116.40	0.15
Longtan	LT	39.88	116.44	0.42
Nanguan	NG	39.94	116.42	0.04
Qingnianhu	QNH	39.95	116.40	0.15
Rendinghu	RDH	39.96	116.38	0.10
Shichahai	SCH	39.94	116.38	0.42
Shuangxiu	SX	39.96	116.37	0.06
Taoranting	TRT	39.87	116.38	0.52
Tiantan	TT	39.88	116.40	1.95
Wanfangyuan	WFY	39.86	116.37	0.12
Wanshou	WS	39.88	116.36	0.04
Xuanwu	XW	39.89	116.35	0.08
Yuyuantan	YYT	39.92	116.32	1.51
Yuetan	YT	39.91	116.35	0.07
Zizhuyuan	ZZY	39.94	116.31	0.42

2.2. Data Sources

Building dataset, Gaofen2 images, and Landsat 8 image were used in this study, as shown in Table 2.

Table 2. Data sources.

Name	Time	Data Types	Scale/Resolution	Data Sources
Building dataset	2015	vector	-	Resources and Environmental Scientific Data Center (RESDC), Chinese Academy of Sciences (CAS)
Gaofen2(GF2) images	2015	Raster	0.61 × 0.61 m	RESDC
Landsat 8 OLI	2015	Raster	30 × 30 m	USGS

Building dataset was derived from Resources and Environmental Scientific Data Center (RESDC), Chinese Academy of Sciences (CAS). It provides building datasets in Chinese major cities, such as Beijing, Tianjin and Jinan. Some parameters, such as building outline and floors, are included in this dataset. It can reflect the two- and three-dimensional characteristics of the building. Taking Baidu Street View map as criteria, 500 samples were randomly selected to verify the accuracy of this dataset. The result shows that the overall accuracy of this dataset was approximately 97%, which can guarantee the accuracy of building classification and subsequent analysis.

The outline of the park was mapped using GF2 images, which were derived from RESDC. To cover the study area, two GF2 images taken on 2 September 2015, and 12 September 2015, respectively, were used in this study, with a panchromatic (spatial resolution of 1 m) and four multi-spectral (blue, green, red, and near infrared, spatial resolutions of 4 m) bands.

To retrieve the LST, two Landsat 8 OLI images were derived from the United States Geological Survey (USGS) on 22 August 2015, and 14 February 2016, respectively. The thermal infrared band (band 10, spatial resolution of 120 m), was used to retrieve the LST. The images were selected to be as cloud-free as possible. Although the cloud cover of this image was 33.33% in summer, the study area was cloud-free.

2.3. Methods

The flowchart of this study is as follows (Figure 2). First of all, the LST was retrieved from two Landast 8 OLI images (summer and winter), and the outline of parks were required by GF2 images. Buildings were classified based on the building dataset. Secondly, the LSTs of parks were calculated, and the LST differences among different parks were analyzed. Thirdly, the CIF of parks were estimated, and CIF of parks were analyzed. Fourthly, average LST of CIFs were calculated, and LST difference between park and CIF were analyzed. Fifthly, the composition of the building neighboring the park was analyzed. Finally, the impacts of neighboring buildings on the CIE of parks was investigated.
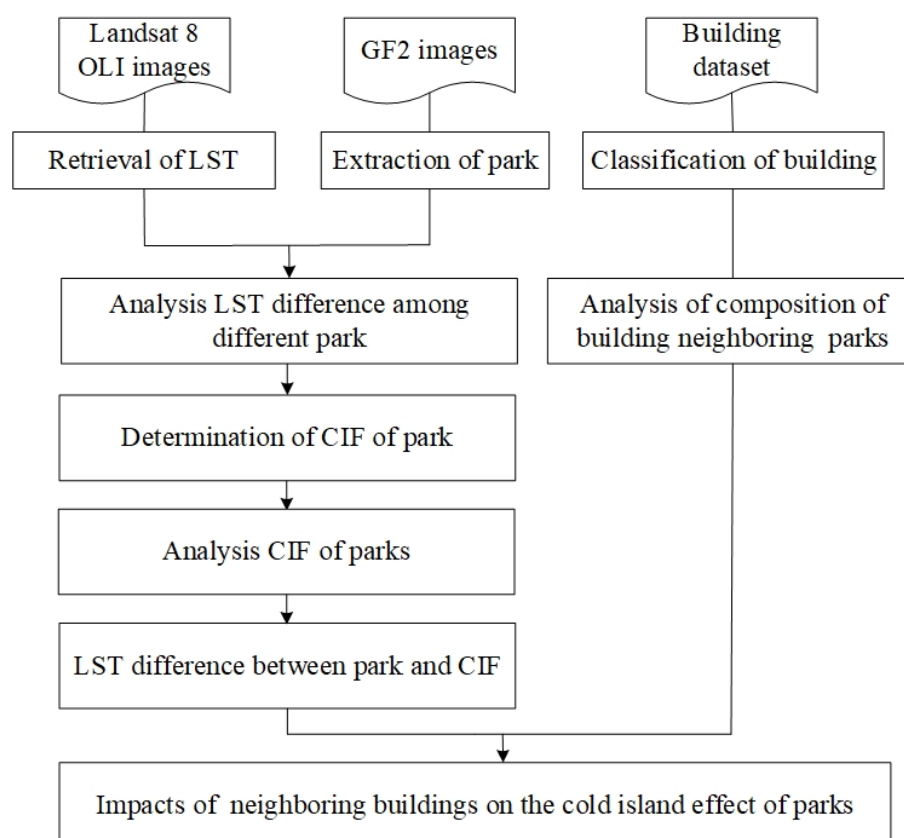

Figure 2. Flowchart of this study.

2.3.1. Retrieval of LST

The image-based method (IBM) is used for retrieval of LST [15]. The equation is as follows

$$T_s = \frac{T}{1 + \left(\frac{\lambda T}{\rho}\right) ln \varepsilon} \tag{1}$$

where T_s is the LST, T represents the at-satellite brightness temperature, λ and ε are the wavelengths at the center of emitted radiance and spectral emissivity, respectively. ρ is a constant value derived from the headed files of the Landsat 8 OLI image. In this case, ρ equals 1.438×10^{-2} mK.

The estimation of T can divide into two steps. First, the digital number (DN) of thermal band (band 10) is converted to radiation. The equation is as follows

$$L\lambda = ML \times DN + AL \tag{2}$$

where $L\lambda$ is the spectral radiance (W·m^{-2}·sr^{-1}·μm^{-1}), ML and AL are rescaled gain (value = 3.342×10^{-4}) and rescaled bias (value = 0.1).

After calculating $L\lambda$, the T can calculate as follows

$$T = \frac{K_2}{ln\left(\frac{K_1}{L\lambda} + 1\right)} \tag{3}$$

where K_1 = 480.89 W·m^{-2}·sr^{-1}·μm^{-1} and K_2 = 1201.14 K.

The estimation of ε can also divide into two steps. First, the land surface is classified into three groups, water, urban, and natural surface. Then, the ε of water is set as 0.995, while for urban and natural surface, the ε can calculate by fractional vegetation cover (FVC) (Equations (4) and (5)). The FVC is calculated by NDVI (Equation (6))

$$\varepsilon_{urban} = 0.9589 + 0.086 FVC - 0.0671 FVC^2 \tag{4}$$

$$\varepsilon_{natural\ surface} = 0.9625 + 0.0614 FVC - 0.0461 FVC^2 \tag{5}$$

$$FVC = \frac{NDVI - NDVI_s}{NDVI_v - NDVI_s} \tag{6}$$

where ε_{urban} and $\varepsilon_{natural\ surface}$ are the emissivity values for urban and natural surface, respectively. *FVC* and *NDVI* are the fractional vegetation cover and Normalized Difference Vegetation Index. $NDVI_s$ and $NDVI_v$ are the NDVI for the vegetation and soil, respectively.

2.3.2. Extraction of Park and Classification of Buildings

The outline of parks was mapped using GF2 images based on the visual interpretation method. Taking TRT as an example, the outline of TRT was extracted based on GF2 images (Figure 3). In this study, twenty-two parks were extracted, and the spatial distribution of parks can be seen in Figure 1.
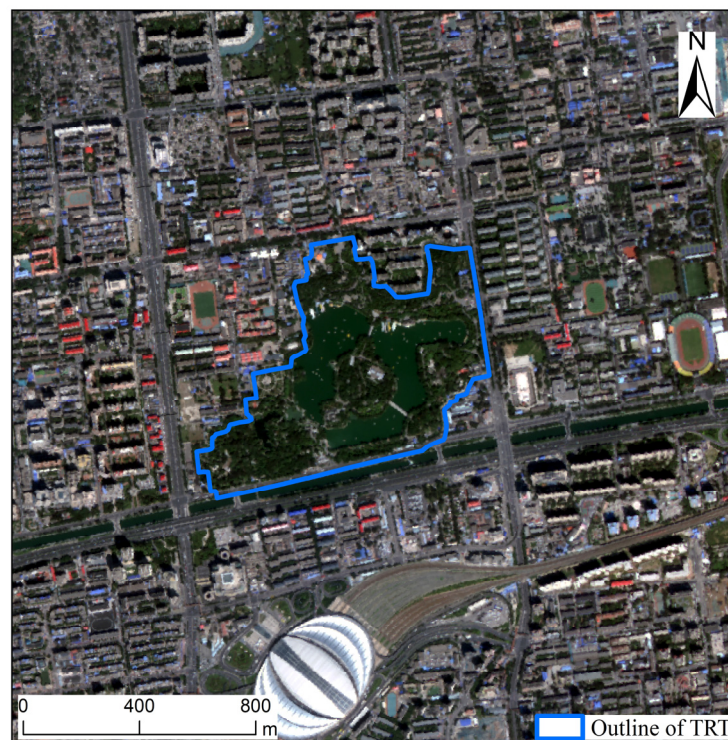
Figure 3. The outline of TRT.

To evaluate the impact of different building types on the CIE of parks, building dataset was used in this study. This dataset includes the outline of the buildings, and the number of building floors. Furthermore, according to Chinese Residential Building Code, buildings were classified into three types based on building floors, including low-rise building (LRB), middle-rise building (MRB), and high-rise building (HRB), respectively. The classification standard can be seen in Table 3.

Table 3. Classification standard of building.

Types	Floors
LRB	1–3
MRB	4–6
HRB	>6

2.3.3. Estimation of CIF

The area where the CIE of parks occurs is defined as the CIF. The greater the CIF, the stronger the park CIE. According to the urban heat island footprint, the buffer method was used to quantitatively measure the CIF of parks [43–45].

Firstly, we constructed buffers of the outline of each park with a distance of 50 m. Then, the mean LST in each buffer were calculated. A scatter plot of the relationship between the buffer number and average LST was drawn. Finally, the CIF of the park was determined by identifying the breakpoint.

Taking TRT as an example, we first constructed buffers of the outline of this park with a distance of 50 m, the buffer diagram is shown in Figure 4. Then, the average LST in each buffer were calculated, and the relationship between the buffer number and average LST was drawn in Figure 5. The result showed that the average LST of TRT is 29.91 °C. As the rings extended outward, the average LST gradually increases, and reached the highest at the fifth rings (35.10 °C). Then, the average LST begins to decrease. Thus, the fifth ring represents the boundary of change in the LST, the area of the five inner rings is determined as the CIF of TRT.
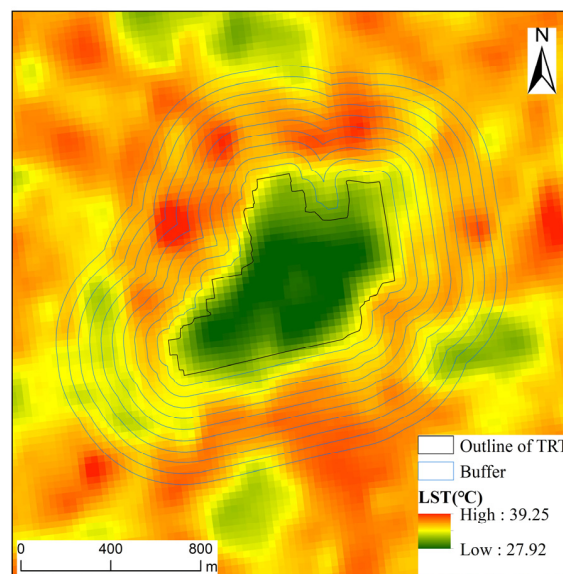
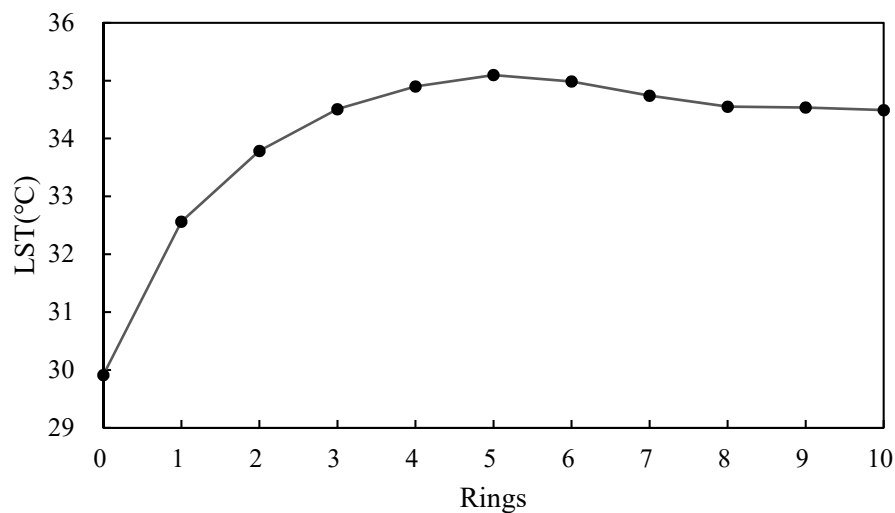**Figure 4.** Buffer diagram in TRT (radius equals 50 m).

Figure 5. Scatter diagram of average LST in rings in TRT.

2.3.4. Analytical Methods

Multiple linear regression model was used to explore the effects of neighboring buildings on CIF of central parks. Three building types, including LRB, MRB and HRB, were also considered in this study. To illustrate the composition and configuration characteristics of buildings, some metrics, including percentage of landscape (PLAND), landscape shape index (LSI), perimeter area fractal dimension (PAFRAC), interspersion juxtaposition index (IJI), and aggregation index (AI), which were quantified by Fragstats 4.2, has been used in this study. Particular, PLAND is used to quantify the composition characteristics of buildings, and LSI, PAFRAC, IJI, and AI are used to quantify the configuration characteristics of buildings.

3. Results

3.1. LST Difference among Different Park

Spatial distribution of LST in the study area is shown in Figure 6. The result shows that the LST of the study area ranged from 19.76 to 43.52 °C in summer, and −20.77 to 8.73 °C in winter. The average LSTs were 33.67 °C in summer and −0.33 °C in winter in the study area. It is obvious

that LSTs of parks are much lower than the neighboring area, indicating that parks are cold islands. Additionally, compared with winter, LSTs of parks in summer are significantly lower than neighboring areas. This indicates that there are large LST differences between parks and neighboring areas in summer compared to winter.
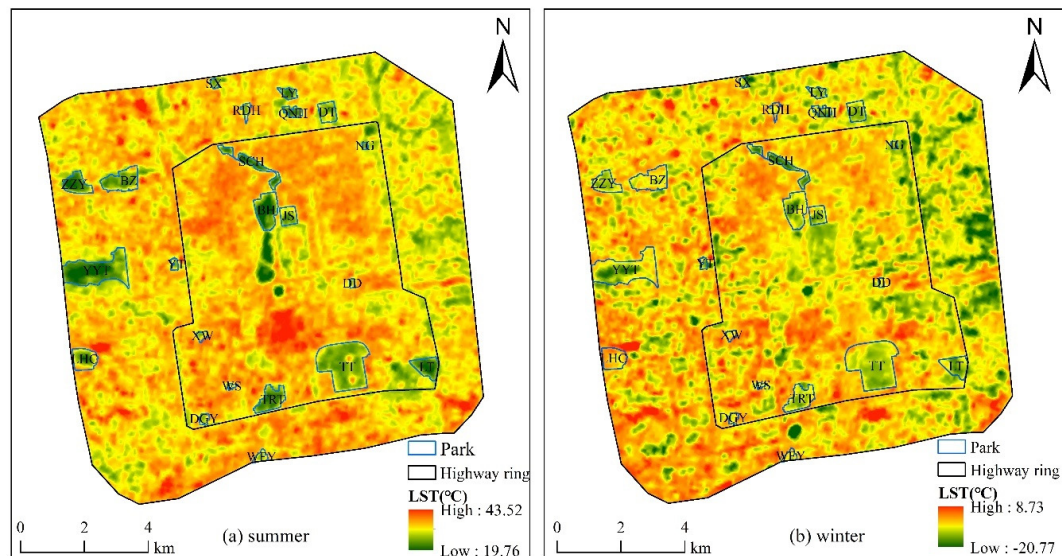

Figure 6. Spatial distribution of LST in the study area.

To further investigate LST differences among different parks, average LSTs of parks in different seasons were calculated (Table 4). In summer, LSTs of parks ranged from 29.25 °C (YYT) to 32.84 °C (WS), with an average LST of 30.98 °C. It is lower than the average LST (33.67 °C) of the study area. Among them, the LST of five parks, including YYT, ZZY, LT, BH, and TRT, is lower than 30 °C. Additionally, the LST of five parks, including WS, XW, WFY, DD, and DGY, is higher than 32 °C. Interestingly, the areas of these five parks are relatively small. In winter, the LST of parks ranged from −2.13 °C (SCH) to 0.29 °C (LHC), with an average LST of −1.10 °C. It should be noted that, except for LHC, the LSTs of other parks are lower than 0 °C. Furthermore, compared with summer, there is little difference in the LSTs of parks.

Table 4. Average LSTs of parks

Park Name	Average LST (°C)	
	Summer	Winter
BH	29.34	−1.46
BZ	30.82	−0.51
DGY	32.05	−0.47
DT	31.35	−1.60
DD	32.28	−0.86
JS	31.42	−1.36
LHC	31.68	0.29
LY	30.16	−1.51
LT	29.34	−1.68
NG	30.81	−1.74
QNH	30.18	−1.62
RDH	31.96	−0.11
SCH	30.08	−2.13
SX	30.85	−1.36
TRT	29.91	−1.19
TT	31.01	−1.34
WFY	32.42	−0.51
WS	32.84	−0.48
XW	32.72	−0.35
YYT	29.25	−1.28
YT	31.75	−1.48
ZZY	29.33	−1.38
Average	30.98	−1.10

3.2. CIF of Parks

The CIF of parks is shown in Figure 7. The results show that the CIF of parks ranged from 0.19 to 3.55 km^2 in summer, and ranged from 0.11 to 1.87 km^2 in winter. The average CIFs were 0.67 in summer and 0.53 km^2 in winter in the study area. In summer, the CIFs of YYT (3.55 km^2), BZ (1.10 km^2), and TRT (1.05 km^2) are large. In contrast, the CIFs of NG, DD, WS, and QNH are small, which are all below 0.30 km^2. It should be noted that the areas of all four parks are small. In winter, the CIF of four parks, including LT (1.87 km^2), YT (1.30 km^2), YYT (1.07 km^2) and TRT (1.05 km^2), is higher than 1 km^2. The CIF of other parks is all below 1 km^2. In particular, the CIF of JS is the smallest (0.11 km^2).
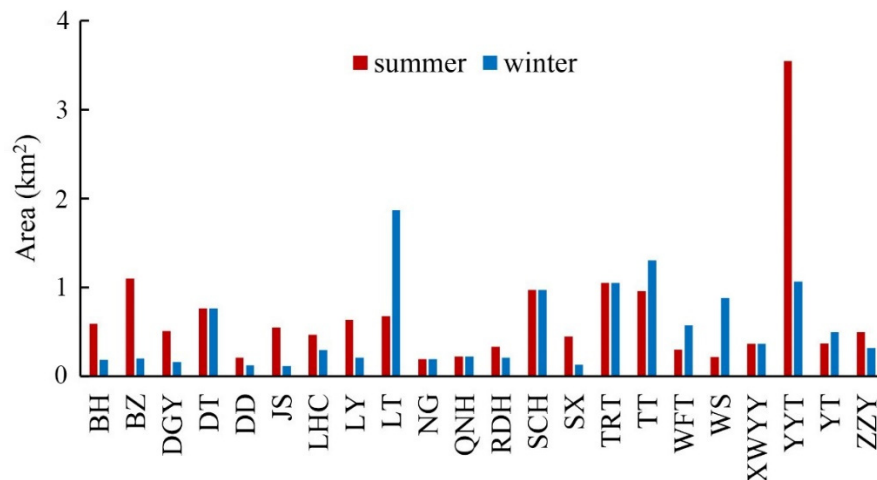

Figure 7. CIF of parks.

The CIF of parks is different in different seasons. In general, the CIF of parks in summer is larger than that in winter, with an average area that is 0.14 km^2 larger. This indicates that the park has a better CIE in summer than that in winter. It is also associated with a lower average temperature in winter. In particular, there are also six parks, such as YRT, SCH, and DT, with consistent CIF in summer and winter. Additionally, the CIFs of five parks, such as LT, WS, and TT, are smaller in summer than in winter.

3.3. LST Difference between Park and CIF

After determining the CIF of parks, the average LSTs of CIFs were also calculated, and LST differences between park and CIF are shown in Table 5. The results show that there is a significant LST difference between park and CIF. The average LST of CIF is higher than that of park, indicating that the LST of parks is lower than in the neighboring area.

Table 5. LST difference between park and CIF.

Park Name	LST Difference (°C)	
	Summer	**Winter**
BH	4.45	1.21
BZ	3.21	0.40
DGY	2.15	0.59
DT	1.90	0.92
DD	2.07	0.51
JS	1.75	0.59
LHC	3.77	0.62
LY	3.39	0.59
LT	3.10	1.10
NG	1.55	0.29
QNH	2.34	0.51

Table 5. *Cont.*

Park Name	LST Difference (°C)	
	Summer	**Winter**
RDH	2.49	0.38
SCH	4.04	1.98
SX	2.76	0.09
TRT	4.29	1.31
TT	3.59	1.71
WFY	1.97	0.80
WS	1.81	0.77
XW	2.31	0.87
YYT	3.79	1.16
YT	2.60	1.40
ZZY	3.75	1.06
Average	2.87	0.86

LST difference between park and CIF ranged from 1.55 °C (NG) to 4.45 °C (BH) in summer, with an average of 2.87 °C. For winter, the LST difference is relatively small, it ranged from 0.09 °C (SX) to 1.98 °C (SCH), with an average of 0.86 °C. Compared with different seasons, the LST difference in summer is higher than that in winter. It also indicated that parks have a strong CIE in summer.

3.4. Composition of Building Neighboring Parks

The compositions of the buildings neighboring parks were calculated, as shown in Figure 8. The results show that the components of the buildings in the CIF of parks are dominated by MRB, followed by LRB, and HRB is the least dominant (Figure 8). The proportion of buildings in the CIF of each park ranged from 14.40% to 35.90% in summer and ranged from 14.23% to 37.58% in winter.
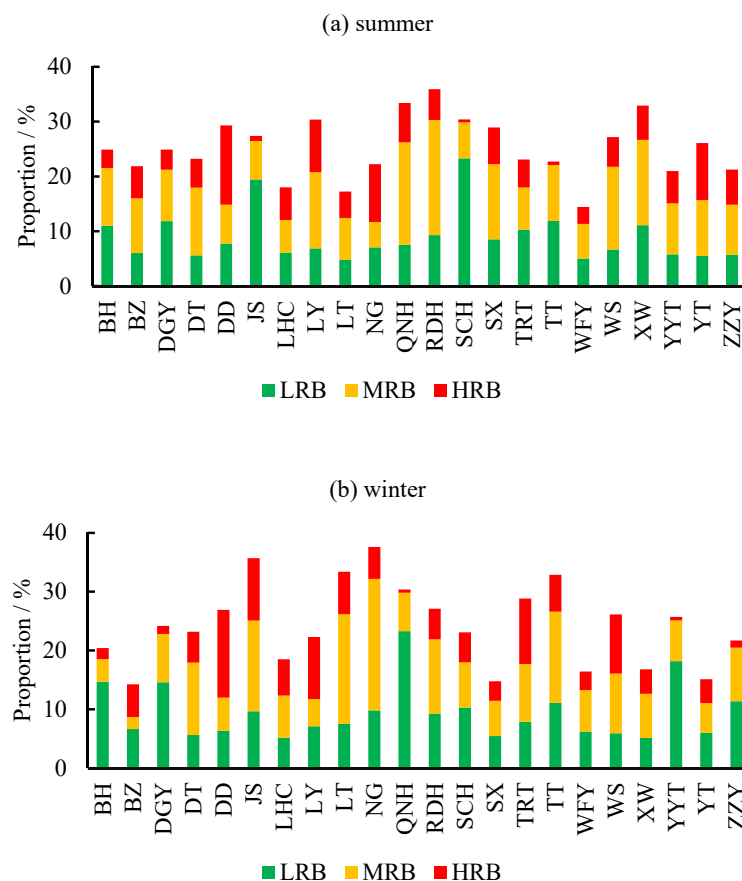

Figure 8. Composition of building types neighboring parks.

In summer, the components of the buildings in the CIF of parks are dominated by MRB, which ranged from 4.62% in NG to 21.00% in RDH (Figure 8a). The proportion of LRB ranged from 4.79% to 23.28%, and the proportion of HRB ranged from 0.53% to 14.44%. For all parks, the neighboring buildings in twelve CIFs are dominated by MRB, such as QNH (18.66%), XW (15.55%), and WS (15.09%), respectively. Additionally, the neighboring buildings in seven CIFs are dominated by LRB, such as QCH (23.28%), JS (19.42%), and TT (11.87%), respectively. Furthermore, the neighboring buildings in three CIFs are dominated by HRB, including DD (14.44%), NG (10.55%), and YT (10.41%).

Similar to summer, the components of the buildings in the CIF of parks are dominated by MRB in winter (Figure 8b). The proportions of MRB, LRB and HRB ranged from 2.04% to 22.35%, 5.11% to 23.26%, and 0.53% to 14.90%. Neighboring buildings in eleven CIFs are dominated by MRB, such as NG (22.35%), LT (18.66%), and TT (15.52%), respectively. Additionally, neighboring buildings in nine CIFs are dominated by LRB, such as QNH (23.26%), YYT (18.16%), and BH (14.68%), respectively. Furthermore, neighboring buildings in two CIFs are dominated by HRB, including DD (14.90%) and TRT (11.16%).

3.5. Impacts of Neighboring Buildings on CIE of Parks

Five metrics, including one composition metric (PLAND), and four configuration metrics (LSI, PAFRAC, IJI and AI), were used to quantitatively investigate the impacts of different types of neighboring buildings on CIE of parks. The impact of composition and configuration variables of buildings on CIE of central parks is shown in Table 6. The results show that there some differences in the key variable between summer and winter. For summer, both composition and configuration variables of MRB, including PLAND and LSI, are significantly related to CIF, suggesting that neighboring MRBs with low density and complex patch shape lead to increased CIE of parks. For winter, only one configuration variable of LRB (PAFRAC) is significantly related to CIF, suggesting that neighboring LRBs with complex patch outline lead to increased CIE of parks.

Table 6. Impacts of composition and configuration variables of buildings on CIF of central parks.

| Season | Building Types | Variables | | | | |
| | | Composition | Configuration | | | |
		PLAND	LSI	PAFRAC	IJI	AI
Summer	LRB	0.29	−0.66	0.18	0.29	0.01
	MRB	−0.54 *	1.60 *	−0.03	−0.27	0.28
	HRB	0.15	−0.11	−0.15	0.06	0.91
Winter	LRB	0.59	−2.12	1.39 *	−0.26	0.40
	MRB	0.40	0.47	−0.76	−0.26	−0.48
	HRB	0.82	1.04	1.21	0.60	0.71

* $p < 0.05$.

4. Discussion

4.1. Scale Effects

IB method was used to retrieve the LST in this study, which has a resolution of 30 m. Inevitably, there are scale effects when carrying out the integration analysis between vector (parks and CIF) and raster data (LST), which can lead to some uncertainties [24]. However, the average area of parks and CIFs are approximately 0.39 and 0.67 km² in summer and 0.53 km² in winter, respectively. This indicates that park LSTs were extracted based on enough LST pixels, which could ensure the accuracy of the results. Furthermore, Liu et al. (2009) pointed out that 30 m was the optimal resolution for investigating the relationship between land use and LST at the patch level in previous studies [46]. Thus, though this may have scale effects, it does not invalidate our results.

4.2. The Relationship between CIF and Park Area

Many studies have pointed out that the CIE of a park is related to its size. In this study, the relationship between the CIF and park area was also evaluated. Figure 9 shows the relationship between CIF and park area. The result shows that the CIF has a positive relationship with park area. This result is consistent with other research [24].
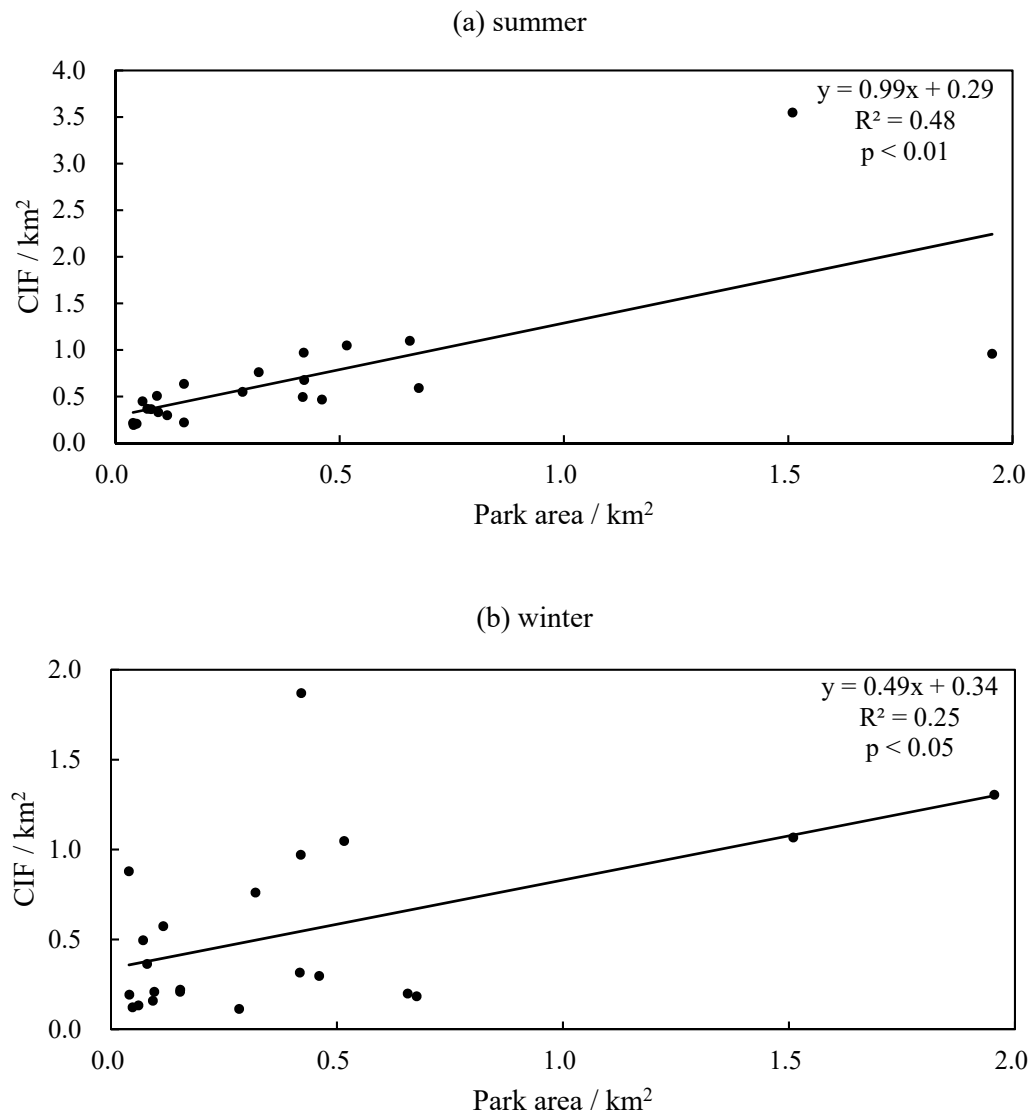
(a) summer

(b) winter

Figure 9. The relationship between cool island footprint and park area.

Regardless of summer and winter, the CIF has a positive relationship with park area, indicating that the larger the park area, the better the CIE. 48% (summer) and 25% (winter) of CIF variation can be explained by park area, and both models passed the significance test. Compared with different seasons, the result also shows that parks have a stronger CIE in summer than that in winter. This is mainly related to the LST differences between parks and neighboring area in winter.

4.3. Implications for Designing Buildings Neighboring the Park for Urban Cooling

Urban parks are considered an effective measure to mitigate the UHI effects [24,31,34]. However, the CIE varied in shape, size, interior components, and neighboring environments [24,33]. Due to rapid urbanization, urban surface elements, especially three-dimensional buildings, have changed

drastically, resulting in changes in urban regional climate [41]. It inevitably has effects on the CIE of parks.

The composition and configuration of neighboring buildings affect the park's CIE. However, the influence is different in different building types. Thus, we suggest that the spatial composition and configuration of the buildings neighboring parks should be emphasized. For MRB, the lower the density and more complex the patch shape, the higher contribution they make to increased CIF in summer. Particularly, due to the high building density and uniform distribution of MRB, it can be considered as the key heat source [38]. For LRB, the more complex patch outline, the higher the contribution they make to increased CIF in winter. Although high building density of LRB in few CIFs can absorb and emit a lot of energy, the density of LRB in most of CIFs are relatively low. Unlike LRB and MRB, HRB can create more shade, and large interval of HRB also can be beneficial for ventilation [11,27,38,47]. However, there is no significant contribution to CIF in different seasons. Given that the UHI effect is strongest in summer, the CIF is relatively small in winter. Thus, reasonable planning of the density and shape of MRB neighboring parks should be taken into account in the future, which can be a key factor to increase the CIE of parks.

4.4. Limitations

In this study, the impacts of neighboring buildings on CIE of parks were explored during summer and winter daytimes. However, due to a lack of nighttime LST data, the impacts and diurnal variation could not be explored. Additionally, this study was carried out in the Beijing metropolitan area, and results may vary in different cities (e.g., coastal cities and industrial cities) or climate conditions (e.g., tropical monsoon climate and subtropical monsoon climate). Therefore, other cities should be further investigated. Furthermore, this study focuses on characterizing the impacts of neighboring buildings on the CIE of central parks. However, many other landscape factors in CIF, including vegetation, pavements and water, can affect a park's CIE. These factors should be considered in future research to comprehensively understand the impacts.

5. Conclusions

This study investigated the impacts of neighboring building on the CIE of central parks based on Landsat 8 OLI images, GF2 images, and building dataset. The key characteristics of buildings which influence parks' CIE were identified in summer and winter. Thus, this study could extend scientific understanding of degree to which CIE of central parks are affected by neighboring buildings (especially different types of buildings), and could provide guidance to urban planners on how to mitigate the UHI effects through the rational allocation of buildings.

The average LSTs of parks are 30.98 °C in summer and −1.10 °C in winter, respectively. LSTs of parks in summer are significantly lower than neighboring areas. CIF of parks in summer is higher than that in winter, with an average area of 0.15 km^2 larger than that in winter. Average LST differences between park and CIF are 2.87 °C in summer and 0.86 °C in winter, indicating that parks have a strong CIE in summer. The components of the building in CIF of parks are dominated by MRB, followed by LRB, and HRB is the least dominant. Furthermore, the PLAND and LSI of MRB, and PAFRAC of LRB are significantly related to CIF in summer and winter. This study demonstrated that parks have a stronger CIE in summer than that in winter, which can effectively mitigate the UHI effects. This study also demonstrated that the CIE of parks can vary in different types of neighboring buildings, especially MRB. It is emphasized that reasonable planning of different types of neighboring buildings (spatial composition and configuration) should be designed based on the characteristics of parks in the future. Our findings are a good theoretical contribution to the urban thermal environment research, providing useful guidance on optimizing buildings for urban planners and administrators. The findings can provide new insights into further exploration of how to improve the CIE of parks.

References

1. Dai, Z.; Guldmann, J.-M.; Hu, Y. Thermal impacts of greenery, water, and impervious structures in Beijing's Olympic area: A spatial regression approach. *Ecol. Indic.* **2019**, *97*, 77–88. [CrossRef]

2. Hasan, S.; Shi, W.; Zhu, X.; Abbas, S. Monitoring of Land Use/Land Cover and Socioeconomic Changes in South China over the Last Three Decades Using Landsat and Nighttime Light Data. *Remote Sens.* **2019**, *11*, 1658. [CrossRef]

3. Liu, J.; Kuang, W.; Zhang, Z.; Xu, X.; Qin, Y.; Ning, J.; Zhou, W.; Zhang, S.; Li, R.; Yan, C.; et al. Spatiotemporal characteristics, patterns, and causes of land-use changes in China since the late 1980s. *J. Geogr. Sci.* **2014**, *24*, 195–210. [CrossRef]

4. Wang, Y.C.; Hu, B.K.H.; Myint, S.W.; Feng, C.C.; Chow, W.T.L.; Passy, P.F. Patterns of land change and their potential impacts on land surface temperature change in Yangon, Myanmar. *Sci. Total Environ.* **2018**, *643*, 738–750. [CrossRef] [PubMed]

5. Yao, R.; Wang, L.; Huang, X.; Niu, Z.; Liu, F.; Wang, Q. Temporal trends of surface urban heat islands and associated determinants in major Chinese cities. *Sci. Total Environ.* **2017**, *609*, 742–754. [CrossRef] [PubMed]

6. Oke, T.R. The energetic basis of the urban heat island. *Q. J. R. Meteorol. Soc.* **1982**, *108*, 1–24. [CrossRef]

7. Rizwan, A.M.; Dennis, L.Y.C.; Liu, C. A review on the generation, determination and mitigation of Urban Heat Island. *J. Environ. Sci.* **2008**, *20*, 120–128. [CrossRef]

8. Mohan, M.; Kandya, A. Impact of urbanization and land-use/land-cover change on diurnal temperature range: A case study of tropical urban airshed of India using remote sensing data. *Sci. Total Environ.* **2015**, *506–507*, 453–465. [CrossRef]

9. Qiao, Z.; Tian, G.; Xiao, L. Diurnal and seasonal impacts of urbanization on the urban thermal environment: A case study of Beijing using MODIS data. *ISPRS J. Photogramm. Remote Sens.* **2013**, *85*, 93–101. [CrossRef]

10. Zhou, D.; Xiao, J.; Bonafoni, S.; Berger, C.; Deilami, K.; Zhou, Y.; Frolking, S.; Yao, R.; Qiao, Z.; Sobrino, J. Satellite Remote Sensing of Surface Urban Heat Islands: Progress, Challenges, and Perspectives. *Remote Sens.* **2018**, *11*, 48. [CrossRef]

11. Qiao, Z.; Xu, X.; Luo, W.; Wang, F.; Luo, L.; Sun, Z. Urban ventilation network model: A case study of the core zone of capital function in Beijing metropolitan area. *J. Clean. Prod.* **2017**, *168*, 526–535. [CrossRef]

12. Wang, Y.; Du, H.; Xu, Y.; Lu, D.; Wang, X.; Guo, Z. Temporal and spatial variation relationship and influence factors on surface urban heat island and ozone pollution in the Yangtze River Delta, China. *Sci. Total Environ.* **2018**, *631–632*, 921–933. [CrossRef] [PubMed]

13. Wang, K.; Jiang, S.; Wang, J.; Zhou, C.; Lee, X. Comparing the Diurnal and Seasonal Variabilities of Atmospheric and Surface Urban Heat Islands Based on the Beijing Urban Meteorological Network. *J. Geophys. Res. Atmos.* **2017**, *122*, 2131–2154. [CrossRef]

14. Doick, K.J.; Peace, A.; Hutchings, T.R. The role of one large greenspace in mitigating London's nocturnal urban heat island. *Sci. Total Environ.* **2014**, *493*, 662–671. [CrossRef]

15. Weng, Q.; Lu, D.; Schubring, J. Estimation of land surface temperature–vegetation abundance relationship for urban heat island studies. *Remote Sens. Environ.* **2004**, *89*, 467–483. [CrossRef]

16. Yang, J.; Wang, Y.; Xiao, X.; Jin, C.; Xia, J.; Li, X. Spatial differentiation of urban wind and thermal environment in different grid sizes. *Urban Clim.* **2019**, *28*, 100458. [CrossRef]

17. Qiao, Z.; Liu, L.; Qin, Y.; Xu, X.; Wang, B.; Liu, Z. The Impact of Urban Renewal on Land Surface Temperature Changes: A Case Study in the Main City of Guangzhou, China. *Remote Sens.* **2020**, *12*, 794. [CrossRef]

18. Yang, J.; Zhan, Y.; Xiao, X.; Xia, J.C.; Sun, W.; Li, X. Investigating the diversity of land surface temperature characteristics in different scale cities based on local climate zones. *Urban Clim.* **2020**, *34*, 100700. [CrossRef]

19. Yin, C.H.; Yuan, M.; Lu, Y.P.; Huang, Y.P.; Liu, Y.F. Effects of urban form on the urban heat island effect based on spatial regression model. *Sci. Total Environ.* **2018**, *634*, 696–704. [CrossRef]

20. Yang, J.; Sun, J.; Ge, Q.; Li, X. Assessing the impacts of urbanization-associated green space on urban land surface temperature: A case study of Dalian, China. *Urban For. Urban Green.* **2017**, *22*, 1–10. [CrossRef]

21. Chang, C.R.; Li, M.H. Effects of urban parks on the local urban thermal environment. *Urban For. Urban Green.* **2014**, *13*, 672–681. [CrossRef]

22. Yan, H.; Wu, F.; Dong, L. Influence of a large urban park on the local urban thermal environment. *Sci. Total Environ.* **2018**, *622–623*, 882–891. [CrossRef] [PubMed]

23. Declet-Barreto, J.; Brazel, A.J.; Martin, C.A.; Chow, W.T.L.; Harlan, S.L. Creating the park cool island in an inner-city neighborhood: Heat mitigation strategy for Phoenix, AZ. *Urban Ecosyst.* **2013**, *16*, 617–635. [CrossRef]

24. Xu, X.L.; Cai, H.Y.; Qiao, Z.; Wang, L.; Jin, C.; Ge, Y.N.; Wang, L.Y.; Xu, F.J. Impacts of park landscape structure on thermal environment using QuickBird and Landsat images. *Chin. Geogr. Sci.* **2017**, *27*, 818–826. [CrossRef]

25. Gunawardena, K.R.; Wells, M.J.; Kershaw, T. Utilising green and bluespace to mitigate urban heat island intensity. *Sci. Total Environ.* **2017**, *584*, 1040–1055. [CrossRef]

26. He, B.-J. Potentials of meteorological characteristics and synoptic conditions to mitigate urban heat island effects. *Urban Clim.* **2018**, *24*, 26–33. [CrossRef]

27. He, B.-J.; Ding, L.; Prasad, D. Enhancing urban ventilation performance through the development of precinct ventilation zones: A case study based on the Greater Sydney, Australia. *Sustain. Cities Soc.* **2019**, *47*, 101472. [CrossRef]

28. Yang, J.; Wang, Y.; Xiu, C.; Xiao, X.; Xia, J.; Jin, C. Optimizing local climate zones to mitigate urban heat island effect in human settlements. *J. Clean. Prod.* **2020**, *275*, 123767. [CrossRef]

29. Yang, J.; Jin, S.; Xiao, X.; Jin, C.; Xia, J.; Li, X.; Wang, S. Local climate zone ventilation and urban land surface temperatures: Towards a performance-based and wind-sensitive planning proposal in megacities. *Sustain. Cities Soc.* **2019**, *47*, 101487. [CrossRef]

30. Chang, C.R.; Li, M.-H.; Chang, S.-D. A preliminary study on the local cool-island intensity of Taipei city parks. *Landsc. Urban Plan.* **2007**, *80*, 386–395. [CrossRef]

31. Feyisa, G.L.; Dons, K.; Meilby, H. Efficiency of parks in mitigating urban heat island effect: An example from Addis Ababa. *Landsc. Urban Plan.* **2014**, *123*, 87–95. [CrossRef]

32. Xiao, X.D.; Dong, L.; Yan, H.N.; Yang, N.; Xiong, Y.M. The influence of the spatial characteristics of urban green space on the urban heat island effect in Suzhou Industrial Park. *Sustain. Cities Soc.* **2018**, *40*, 428–439. [CrossRef]

33. Lin, W.; Yu, T.; Chang, X.; Wu, W.; Zhang, Y. Calculating cooling extents of green parks using remote sensing: Method and test. *Landsc. Urban Plan.* **2015**, *134*, 66–75. [CrossRef]

34. Dai, Z.X.; Guldmann, J.M.; Hu, Y.F. Spatial regression models of park and land-use impacts on the urban heat island in central Beijing. *Sci. Total Environ.* **2018**, *626*, 1136–1147. [CrossRef] [PubMed]

35. Han, D.; Yang, X.; Cai, H.; Xu, X.; Qiao, Z.; Cheng, C.; Dong, N.; Huang, D.; Liu, A. Modelling spatial distribution of fine-scale populations based on residential properties. *Int. J. Remote Sens.* **2019**, *40*, 5287–5300. [CrossRef]

36. Liu, C.; Huang, X.; Wen, D.; Chen, H.; Gong, J. Assessing the quality of building height extraction from ZiYuan-3 multi-view imagery. *Remote Sens. Lett.* **2017**, *8*, 907–916. [CrossRef]

37. Yang, J.; Su, J.; Xia, J.; Jin, C.; Li, X.; Ge, Q. The Impact of Spatial Form of Urban Architecture on the Urban Thermal Environment: A Case Study of the Zhongshan District, Dalian, China. *IEEE J. Sel. Top. Appl. Earth Obs. Remote Sens.* **2018**, 1–8. [CrossRef]

38. Feng, X.; Myint, S.W. Exploring the effect of neighboring land cover pattern on land surface temperature of central building objects. *Build. Environ.* **2016**, *95*, 346–354. [CrossRef]

39. Yang, X.; Li, Y. The impact of building density and building height heterogeneity on average urban albedo and street surface temperature. *Build. Environ.* **2015**, *90*, 146–156. [CrossRef]

40. Schrijvers, P.J.C.; Jonker, H.J.J.; Kenjeres, S.; de Roode, S.R. Breakdown of the night time urban heat island energy budget. *Build. Environ.* **2015**, *83*, 50–64. [CrossRef]

41. Cai, H.; Xu, X. Impacts of Built-Up Area Expansion in 2D and 3D on Regional Surface Temperature. *Sustainability* **2017**, *9*, 1862. [CrossRef]

42. Guo, A.; Yang, J.; Xiao, X.; Xia, J.; Jin, C.; Li, X. Influences of urban spatial form on urban heat island effects at the community level in China. *Sustain. Cities Soc.* **2020**, *53*, 101972. [CrossRef]

43. Qiao, Z.; Wu, C.; Zhao, D.; Xu, X.; Yang, J.; Feng, L.; Sun, Z.; Liu, L. Determining the Boundary and Probability of Surface Urban Heat Island Footprint Based on a Logistic Model. *Remote Sens.* **2019**, *11*, 1368. [CrossRef]

44. Zhao, M.Y.; Cai, H.Y.; Qiao, Z.; Xu, X.L. Influence of urban expansion on the urban heat island effect in Shanghai. *Int. J. Geogr. Inf. Sci.* **2016**, *30*, 2421–2441. [CrossRef]

45. Zhou, D.C.; Zhao, S.Q.; Zhang, L.X.; Sun, G.; Liu, Y.Q. The footprint of urban heat island effect in China. *Sci. Rep.* **2015**, *5*. [CrossRef]

46. Liu, H.; Weng, Q. Scaling Effect on the Relationship between Landscape Pattern and Land Surface Temperature. *Photogramm. Eng. Remote Sens.* **2009**, *75*, 291–304. [CrossRef]

47. He, B.-J.; Ding, L.; Prasad, D. Wind-sensitive urban planning and design: Precinct ventilation performance and its potential for local warming mitigation in an open midrise gridiron precinct. *J. Build. Eng.* **2019**, *29*, 101145. [CrossRef]

Publisher's Note: MDPI stays neutral with regard to jurisdictional claims in published maps and institutional affiliations.